Macromolecules

Article

pubs.acs.org/Macromolecules

Crystal Structure and Molecular Packing Behavior of Poly(2,3-diphenyl-1,4-phenylenevinylene) Derivatives Containing Alkyl Side-Chains

Xiang-Kui Ren,[†] Yu-Chun Wu,[‡] Shao-Jie Wang,[†] Shi-Dong Jiang,[§] Jun-Feng Zheng,[†] Shuang Yang,[†] Er-Qiang Chen,*[,†] Chien-Lung Wang,[‡] and Chain-Shu Hsu*[,‡]

[†]Beijing National Laboratory for Molecular Sciences, Department of Polymer Science and Engineering and Key Laboratory of Polymer Chemistry and Physics of Ministry of Education, College of Chemistry, Peking University, Beijing 100871, China

[‡]Department of Applied Chemistry, National Chiao Tung University, Hsin-Chu, 30010 Taiwan

[§]Technical Institute of Physics and Chemistry, Chinese Academy of Sciences, Beijing 100190, China

Supporting Information

ABSTRACT: Phase behavior and crystal structure of a series of poly(2,3-diphenyl-5-alkyl-*p*-phenylenevinylene) (denoted as DP*n*-PPV, where *n* represents the carbon number of the alkyl side-chain, *n* = 6, 8, 10, 12) were studied using differential scanning calorimetry, one- and two-dimensional (1D and 2D) wide-angle X-ray diffraction (WAXD), and selected area electron diffraction (SAED). The experimental results reveal that DP*n*-PPV exhibits one crystalline phase at low temperatures. On the basis of 2D WAXD and SAED patterns obtained from the oriented samples, the crystal structures are determined to be orthorhombic for DP6-PPV and monoclinic for DP8-PPV, DP10-PPV, and DP12-PPV. To account for the unusually large unit cell dimensions, we propose that the unit cell of DP*n*-PPV contains 4 chains (8 chemical repeat units). The complex crystal structure can be attributed to the longitudinal and transverse offsets between the neighboring chains, which shall be mainly due to the requirement of minimizing the steric hindrance caused by the attached pendent groups and maximizing the $\pi-\pi$ interaction between the chains. The molecular packing scheme was simulated by using Cerius[2] software, of which the result agrees with the experimental data. The polarized UV−vis absorption and polarized solid-state photoluminescence (PL) property of these polymers was also investigated. The PL spectra indicated that the light emitted from the oriented film was preferentially polarized parallel to the shear direction, implying that DP*n*-PPV may potentially be useful in linearly polarized luminescence devices.

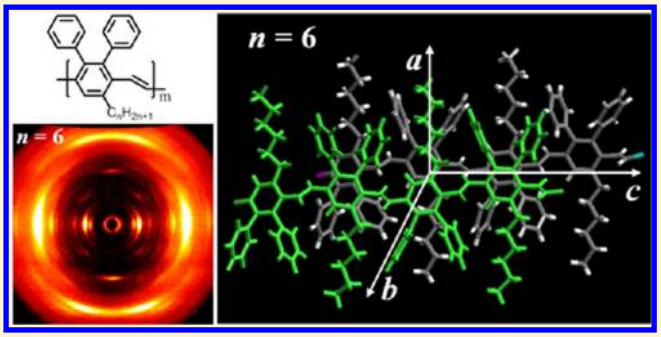

INTRODUCTION

Conjugated polymers have gained much interest because of their unique electrical and photonic semiconducting properties which may be useful in various optoelectronic applications such as light-emitting diodes (LED),[1−4] thin film transistors,[5] all-optical switcher,[6] and organic solar cells.[7] Among them, poly(phenylenevinylene) (PPV) and its derivatives have been extensively studied.[8] For the purposes of enhancement of light-emitting efficiency, color tuning, upgrading of device performance and improvement of solubility, a wide range of PPV derivatives with different conjugation length and side groups have been synthesized. It has also been demonstrated that PPV derivatives can provide linearly polarized emission,[9−14] which may facilitate the fabrication of liquid crystal displays without polarizer and thus, lead to simplification of display manufacture and reduction of cost.

It is known that the photophysical properties of PPV derivatives in solid state are strongly influenced by their chain conformation and chain packing behavior. To understand the relationship between phase structure and photophysical property, crystal structures of PPV and many of its derivatives have been carefully investigated by means of X-ray diffraction and electron diffraction methods.[15−31] It is found that the extended PPV chains, as originally reported by Gagnon et al.,[15] can be well aligned along the stretching direction, with a repeat unit length of 0.66 nm that is identical to the theoretical value.[16] A detailed electron diffraction study of PPV undertaken by Granier et al. reveals that unsubstituted PPV has a monoclinic unit cell with dimensions of a = 0.79 nm, b = 0.61 nm, c = 0.66 nm, and α = 123°.[17] The same report also states that there is a herringbone arrangement of PPV chains with two chains per unit cell. Afterward, these lattice parameters and chain arrangement have been confirmed with some minor refinements.[18−20] For PPV derivatives, it is found

Received: October 4, 2012
Revised: November 29, 2012
Published: December 14, 2012

that even bearing relatively large side groups the polymers can remain semicrystalline.[21−26] However, the addition of side groups can greatly change the crystal structure in comparison with that of the pristine PPV.[27−29] For instance, the crystal structure of poly(2-methyloxy-5-ethylhexyloxyphenylenevinylene) (MEH-PPV) and poly(2,5-di(2′-ethylhexyloxy)-1,4-phenylenevinylene) (DEH-PPV) is determined to be orthorhombic and tetragonal with two chains per unit cell, respectively.[30,31]

Although considerable progress in chemical modifications has been made toward achieving outstanding optoelectronic properties of PPV-based materials, poor solid-state photoluminescence (PL) efficiency remains a long-lasting challenge. To overcome this obstacle, a new family of soluble PPV, namely, poly(2,3-diphenylphenylenevinylene) (DP-PPV) and its derivatives were synthesized with the solid-state PL efficiency higher than 60%.[32,33] Recently, we have also reported various types of novel DP-PPV derivatives[34,35] and DP-PPV-based copolymers[36−38] which can render excellent polymer light emitting diode performance. Similar to other PPV-based polymers, the PL properties of DP-PPV derivatives are also strongly dependent on their assembly behavior. Although the chain aggregation of DP-PPVs in solutions has been studied both experimentally and theoretically,[39−41] the crystal structure and molecular packing behavior of DP-PPVs in the bulk state are not well explored. Therefore, in order to obtain better understanding of the structure−property relationships, it is necessary to elucidate the crystal structure.

In this article, we report the phase behavior and crystal structure of a series of DP-PPV derivative, poly(2,3-diphenyl-5-alkyl-*p*-phenylenevinylene) (denoted as DP*n*-PPV, where *n* represents the carbon number of the alkyl side-chain, n = 6, 8, 10, 12, see Chart 1). The phase behavior and crystal structure

Chart 1. Chemical Structure of DP*n*-PPV, n = 6, 8, 10, 12

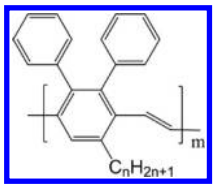

of DP*n*-PPV were determined using differential scanning calorimetry (DSC), one- and two-dimensional (1D and 2D) wide-angle X-ray diffraction (WAXD), and selected area electron diffraction (SAED). The molecular packing scheme of the polymers was simulated by using Cerius^2 software, of which the results agree with the experimental observations. Different from that other PPV polymers possess two chains per unit cell, the unit cell of all the four DP*n*-PPVs studied contains 4 chains (8 chemical repeat units). While DP6-PPV adopts an orthorhombic unit cell, the rest three samples possess monoclinic unit cells. The extended DP*n*-PPV chains are more or less lath-like and parallel stack with each other. However, the steric demands of the attached phenyl rings and alkyl side-chains and the maximization of $\pi-\pi$ interaction between the chains cause the longitudinal and transverse offsets between the neighboring chains of these DP*n*-PPVs, resulting in the unusually large lattice dimensions. We also investigated preliminarily the linearly polarized PL properties of the orientated DP*n*-PPV films. The dichroic ultraviolet−visible (UV−vis) absorption and polarized PL spectra of the four DP*n*-PPV samples indicate that the light emitted from the oriented film is preferentially polarized parallel to the shear direction which is along the chain axis, implying that the polymers have the potential for linearly polarized luminescence device applications.

EXPERIMENTAL SECTION

Materials and Sample Preparation. The DP*n*-PPV samples were synthesized according to the procedure described elsewhere,[32,34] of which the chemical structure was confirmed by various techniques. The number-average molecular weights of the samples are in the range from 100 to 300 kDa with a polydispersity of ∼2.6 which were measured by gel permeation chromatography using polystyrene standards.

For DSC measurements, a typical mass of ∼5 mg was encapsulated in a sealed aluminum pan with the pan weight identically matched to the reference pan. The samples of 1D WAXD experiments were cast from chloroform solution and dried at room temperature under a vacuum. The films were then kept under vacuum for several days. The oriented samples were prepared by mechanically shearing the DP6-PPV, DP8-PPV, DP10-PPV, and DP12-PPV at 330, 290, 290, and 280 °C, respectively, followed by fast cooling to room temperature. For PL and polarized light microscopy (PLM) experiment, the samples were oriented on the quartz plate and on the slide glass, respectively. For transmission electron microscopy (TEM) and UV−vis absorption studies, thin films were prepared by casting a dilute chloroform solution (0.05%, w/v) on the cover glass and the quartz plate, respectively. Orientation of thin film was achieved by mechanical shearing. Before transferred to TEM copper grids, the thin film was coated with carbon and then detached from the substrate using aqueous HF solutions.

Equipment and Experiments. DSC measurements were carried out utilizing a PerkinElmer Pyris I with a mechanical refrigerator. The temperature and heat flow were calibrated at different heating and cooling rates (1−40 °C/min) using standard materials such as benzoic acid and indium. 1D WAXD experiments were performed on a Philips X'Pert Pro diffractometer with a 3 kW ceramic tube as the X-ray source (Cu Kα) and an X'celerator detector. The sample stage was set horizontally. The reflection peak positions were calibrated with silicon powder ($2\theta > 15°$) and silver behenate ($2\theta < 10°$). A temperature control unit (Paar Physica TCU 100) in conjunction with the diffractometer was utilized to study the structure evolution of DP*n*-PPV as a function of temperature. The average heating and cooling rate was 1.5 °C/min. 2D WAXD patterns were obtained using a Bruker D8Discover diffractometer with a GADDS as the 2D detector. Again, calibration was conducted using silicon powder and silver behenate. The oriented samples were mounted on the sample stage with the point-focused X-ray beam aligned perpendicular to the shear direction. The 2D diffraction pattern was recorded in a transmission mode at room temperature. The background scattering was recorded and subtracted from the sample pattern. The crystal unit cell determination procedure was based on construction of the reciprocal lattice. First, all the diffraction spots observed from the fiber pattern were fit into a lattice with six parameters of the unit cell dimensions (a, b, c, and α, β, γ) by hand calculation. Afterward, all the experimental data and calculated data were input into a computer program of refinement. Starting with the unit cell shape and size obtained based on the hand calculation, a continuous computer refinement was conducted to achieve the fit with the least error between experimental results and calculated data.[42]

TEM experiments were carried out with a JEOL JEM-2100 using an accelerating voltage of 200 kV. The d-spacings were calibrated using a TlCl standard. PLM observation was performed on a Leica DML microscope. For density measurements, an aqueous solution of potassium iodide was used to find the density of crystallized fiber samples. The measured density value was used to judge the number of chemical repeating units in the crystalline unit cell. Polarized UV−vis absorption spectra were recorded on a Hitachi U-4100 spectrometer with a polarizer inserted between the sample and the light source

dx.doi.org/10.1021/ma302082x | *Macromolecules* 2013, 46, 155−163

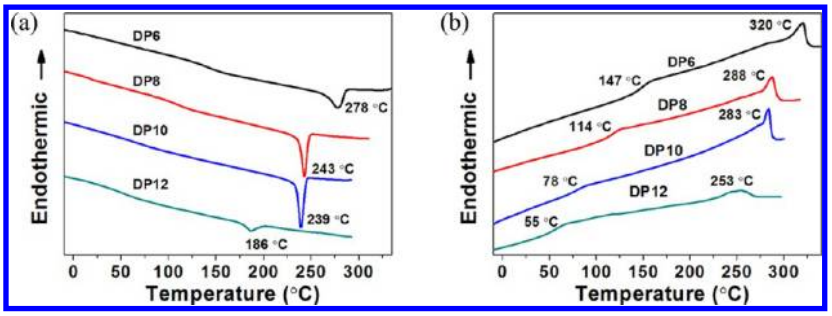

Figure 1. DSC traces of the four DP*n*-PPV samples recorded upon cooling (a) and subsequent heating (b) at a rate of 10 °C/min.

parallel or perpendicular to the shear direction. The dichroic ratio of absorption is defined as $D_{abs} = A_{\parallel}/A_{\perp}$, where $A_{\parallel}$ and $A_{\perp}$ are the absorption of light parallel and perpendicular to the shear direction, respectively. The polarized PL spectra were measured on a Hitachi F4500 fluorescence spectrometer with a Glan-Thompson polarized prism inserted between the sample and the light source. The excitation light was fixed at a wavelength of λ_{ex} = 360 nm and the slits with band-pass of 5 nm were used for both monochromators. The dichroic ratio of PL is defined as $D_{PL} = I_{\parallel}/I_{\perp}$, where $I_{\parallel}$ and $I_{\perp}$ are the emission intensities of the lights emitting parallel and perpendicular to the shear direction, respectively.

Molecular Modeling. Molecular modeling and simulation of the diffraction patterns were performed using the Cerius[2] package of Accelrys. The global equilibrium conformation of DP*n*-PPV was constructed at 0 K using the COMPASS force field. The polymer chain with the lowest energy was chosen as the starting conformation. Basic unit cell parameters determined by crystallographic experimental data were used to build the crystal unit cell. During simulation, the cell parameters were fixed and the atom positions of DP*n*-PPV were able to be varied in the unit cell. The detailed arrangement of polymer chains was justified by comparing the simulated diffraction with the experimental data of 2D WAXD.

RESULTS AND DISCUSSION

Thermal Properties and Structural Evolutions. Parts a and b of Figure 1 depict DSC diagrams of DP*n*-PPVs (n = 6, 8, 10, 12) obtained during cooling and subsequent heating at a rate of 10 °C/min, respectively. In general, the four samples present a similar enantiotropic phase transition behavior.[43] Upon heating, the samples undergo a glass transition followed by a rather broad endothermic process which should be associated with the crystal melting. The peak temperature of the exotherm observed during cooling is ~50 °C lower than that of the endotherm, indicating that DP*n*-PPV crystallization requires a substantially large undercooling. Similar to that of other rigid rod-like polymer bearing flexible side-chains, both the glass transition temperature (T_g) and the melting temperature (T_m) of DP*n*-PPV decrease with increasing the alkyl side-chain length n. For instance, the values of T_g and T_m (the peak temperature of endotherm) of DP6-PPV are 147 and 320 °C, respectively, but for DP12-PPV, the two temperatures are dramatically decreased to 55 and 253 °C.

The phase transition of DP*n*-PPV was further characterized by thermal 1D WAXD experiments. Figure 2 shows a set of 1D WAXD powder patterns of DP8-PPV recorded at different temperatures during cooling. One crystallization process is observed, in agreement with that shown in the DSC diagram (Figure 1a). At temperatures above 290 °C, DP8-PPV is in the isotropic state. Two amorphous halos can be observed with the scattering maxima located at 2θ around 6.7° (d-spacing of 1.32 nm) and 17.2° (d-spacing of 0.52 nm), respectively. The former one looks similar to that observed in comb-like copolymers and

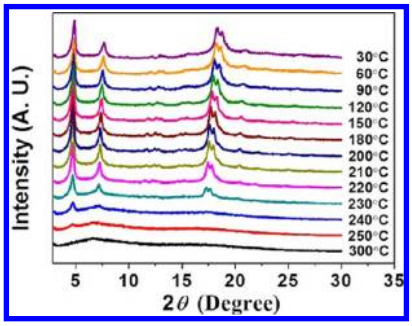

Figure 2. Set of 1D WAXD patterns of DP8-PPV recorded upon cooling from isotropic state.

hairy-rod polymers, which may be partly related to the lateral dimension of polymer chains (e.g., diameter of rod-like chain). The later one should correspond to a liquid-like, short-range order in the disturbed stacking of chains. Decreasing temperature results in crystallization of DP8-PPV, evidenced by the appearance of diffraction peaks in both low- and high-angle region. For instance, at 230 °C, the two rather strong low-angle diffractions are located at 2θ of 4.7° and 7.2°; in the high-angle region, two largely overlapped diffractions peak at 17.3° and 17.6°, respectively. This indicates that the ordering on the two different length scales of nanometer and subnanometer are developed. Further cooling to low temperature causes the continuous shift of diffractions toward higher angles because of the thermal shrinkage. Meanwhile, the diffractions increase in intensity, indicating the increase of crystallinity.

For other three DP*n*-PPVs, a similar process of the phase structure evolution can be observed. Figure 3 shows the 1D WAXD patterns of the four samples at room temperature. In order to obtain high crystallinities, the four samples were slowly cooled from the melt and isothermally annealed for more than 12 h at 200 (DP6-PPV), 170 (DP8-PPV), 130 (DP10-PPV), and 120 °C (DP12-PPV) respectively. Unfortunately, the thermal treatment on these samples in the quiescent state did not result in significant perfections of the crystallinities and the crystallite size. It can be found that the degree of ordering of DP*n*-PPV is highly dependent on the alkyl side-chain length. With increasing n, the number of diffractions which can be unambiguously recognized becomes fewer. For DP10-PPV and DP12-PPV, quiescent cooling from the isotropic state and the isothermal annealing just results in poorly developed crystallinities, and the samples might bear some features of liquid crystal. However, since the backbone chemical structures of the four samples are identical, it is reasonable to presume that they should share similar molecular packing behavior. Those 1D WAXD patterns lack lattice dimensionality of their crystal structures and thus, are not sufficient for a complete

dx.doi.org/10.1021/ma302082x | Macromolecules 2013, 46, 155−163

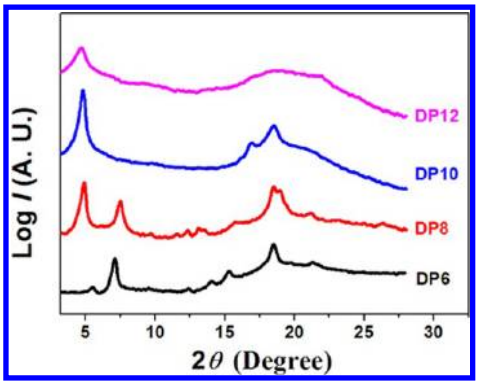

Figure 3. 1D WAXD patterns of the four DP*n*-PPV samples at room temperature. The samples were cooled from the isotropic phase and isothermally annealed for more than 12 h at 200 (DP6-PPV), 170 (DP8-PPV), 130 (DP10-PPV), and 120 (DP12-PPV), respectively, under a dry nitrogen atmosphere.

structure determination. To identify their crystal structure, we focused on the 2D WAXD results of the oriented samples, which will be discussed in great detail below.

Crystal Structure Identification of DP*n*-PPV. Figure 4 presents a series of 2D WAXD patterns of the four DP*n*-PPV

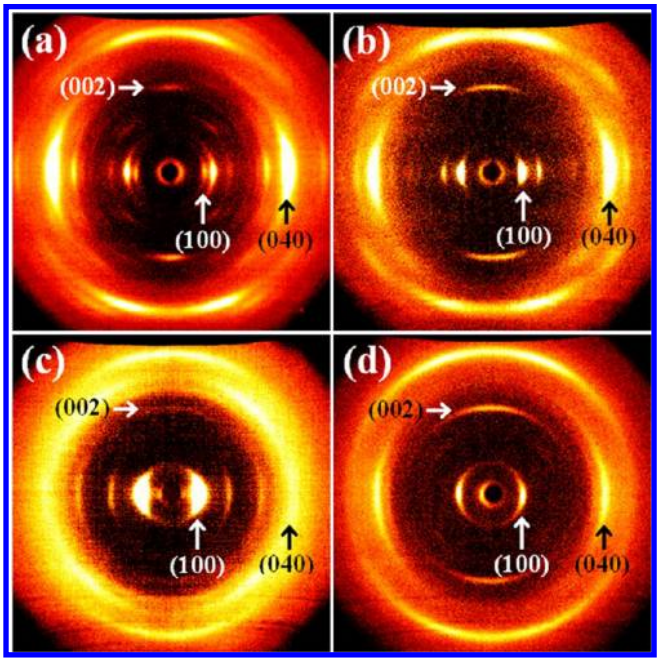

Figure 4. 2D WAXD patterns of the four oriented DP*n*-PPV samples prepared by mechanical shearing recorded at room temperature. The shear direction is on the meridian. (a) $n = 6$, (b) $n = 8$, (c) $n = 10$, and (d) $n = 12$. The (100), (040), and (002) diffractions are indexed in the patterns.

samples oriented by mechanical shearing. The patterns were taken at room temperature with the X-ray incident beam perpendicular to the shear direction which is along the meridian. For each sample, the pattern exhibits diffractions not only on the equator and meridian but also in the quadrants, suggesting an ordered crystal phase. The diffractions detected by 1D WAXD (Figure 3) can also be found in the 2D WAXD patterns. Notably, the mechanical shearing significantly improved the order of chain packing. For example, the diffraction of DP6-PPV located at $2\theta = 5.5°$, which is the first and weak peak in the 1D WAXD pattern (see Figure 3), becomes obvious in the 2D pattern (Figure 4a), appearing on the equator with a medium intensity. Quite a few diffractions with different Miller indices can be identified in some particular positions of the 2D WAXD patterns. In this case, we tried to deduce the crystal structure of DP*n*-PPV.

Figure 4a describes the 2D WAXD pattern of the oriented DP6-PPV. A similar pattern has been reported in ref 34. We reproduced the 2D WAXD experiment many times, and the result with the best quality is presented here. Considering that mechanical shearing with relatively large external force usually aligns the polymer chains along the shear direction, we presume that the *c*-axis of the DP6-PPV is on the meridian. Note that on the meridian there is one diffraction arc at $2\theta = 13.7°$, with the corresponding *d*-spacing of 0.65 nm very close to the (001) unit cell dimension measured for the unsubstituted PPV.[15−31] This observation indicates that the meridional arc should correspond to monomeric repeat dimension along the backbone with the fully extended conformation (see below the result of molecular simulation). Consequently, the *c*- and *c**-axis of DP6-PPV is collinear. The meridianal arc of 0.65 nm is in fact located on the second layer of the diffractions and thus, should be indexed as the (002) with extinctions of the (001) and the (003). Meanwhile, a few diffraction arcs of (*hkl*) with l = odd numbers can be observed in the quadrants. Therefore, we consider that two chemical repeat units of each DP6-PPV chain are included to construct the minimum structural repeat unit of the unit cell.

According to the principles of the reciprocal lattice and diffraction geometry shown in Figure 4a, the *a**- and *b**-axes can be tentatively assumed to be on the equator, namely, the (*hk*0) diffractions are thus on the equator. Since the *c**-axis is along the meridian, the crystal structure is either orthorhombic or monoclinic. Following the standard procedure of determining the crystal lattice,[42,44−46] a triangle of the (*hk*0) diffractions on the equator direction can be constructed. The γ^* angle is calculated to be 90° and all of the (*hk*0) diffractions can be indexed based on the triangle. The diffraction arc at $2\theta = 5.5°$ ($d = 1.61$ nm) is assigned to be the (100). In order to index all the (*hk*0) diffractions of DP6-PPV, we find that the diffraction arc at $2\theta = 18.5°$ ($d = 0.48$ nm), which is the strongest among all of the diffractions, can be assigned as the (040). Using the refinement procedure,[42,44−46] the unit cell of the crystal is finally determined to be orthorhombic one with dimensions of $a = 1.61$ nm, $b = 1.92$ nm, $c = 1.29$ nm, and $\alpha = \beta = \gamma = 90°$, containing 4 chains (8 chemical repeat units). Such a large unit cell dimension is quite remarkable, indicating a complex molecular packing scheme in the unit cell which is probably due to the longitudinal and transverse offsets among the polymer chains (see below the discussion). The experimental and calculated diffraction angles (2θ) and *d*-spacing values of the crystal lattice are listed in Table 1. The calculated crystallographic density is 1.13 g/cm^3, in agreement with the experimental result of 1.10 g/cm^3.

The structural determination of DP6-PPV based on 2D WAXD result can also be supported by SAED experiment conducted on a shear-aligned specimen under TEM. Figure 5a shows the representative bright field morphology of the thin specimen, and Figure 5b is the corresponding SAED pattern. In Figure 5b, there are fewer diffraction arcs than that shown in the 2D WAXD pattern (Figure 4a), probably because of the small selected area of the thin specimen and an incomplete fiber pattern. However, the crystal orientation and diffraction

dx.doi.org/10.1021/ma302082x | *Macromolecules* 2013, 46, 155−163

Table 1. Crystallographic Parameters of DP6-PPV

	2θ (deg)		d-spacing (nm)		intensity	
(hkl) plane	expt[a]	calcd[b]	expt[a]	calcd[b]	expt[c]	simu[d]
100	5.5	5.5	1.61	1.61	m	s
110	7.1	7.2	1.24	1.23	s	s
101	–	8.8	–	1.01	–	w
020	9.3	9.2	0.95	0.96	w	m
111	9.9	9.9	0.90	0.89	w	w
021	11.5	11.5	0.77	0.77	vw	w
002	13.7	13.7	0.65	0.65	m	w
220	14.3	14.4	0.62	0.62	vw	w
130	15.1	14.9	0.59	0.60	m	m
112	15.5	15.5	0.57	0.57	vw	vw
040	18.5	18.5	0.48	0.48	vs	vs
222	19.6	19.9	0.45	0.45	vw	vw
113	21.9	21.8	0.41	0.41	vs	vs
410	23.0	22.6	0.39	0.39	w	w
023	23.0	22.6	0.39	0.39	vw	vw
042	23.1	23.1	0.39	0.39	vw	–

[a]Experimental values observed in Figure 4. [b]Calculated values based on the orthorhombic unit cell of a = 1.61 nm, b = 1.92 nm, c = 1.29 nm, $\alpha = \beta = \gamma = 90°$. [c]The experimental intensities in Figure 4 and. [d]The simulated intensities in Figure 8 are semiquantitatively estimated and classified as very strong (vs), strong (s), medium (m), weak (w), and very weak (vw).

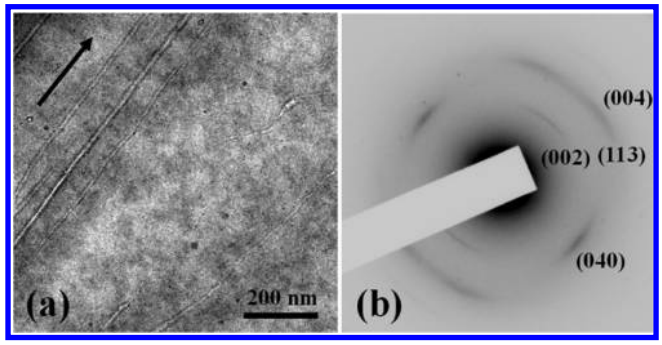

Figure 5. (a) TEM bright field image of the oriented DP6-PPV thin film. The one-way arrow indicates the shear direction. (b) SAED pattern of the oriented film. The well recognized diffraction arcs in the high-angle region are indexed.

symmetry possess better qualities. The SAED pattern can help to index the diffraction arcs and confirm the crystal structure and unit cell dimension obtained by 2D WAXD pattern. The d-spacing values of the (040), (002), (004), and (113) diffractions agree well with the values calculated from the 2D WAXD result.

Compared to the 2D WAXD pattern of oriented DP6-PPV (Figure 4a), Figure 4b of DP8-PPV shows fewer and more diffused diffraction arcs on the equator and in the quadrants, yet the overall diffraction geometry is similar. The chain conformation and packing scheme of DP8-PPV must not be very different from those of DP6-PPV. As shown in Figure 4b, we index again that the meridianal arc of 0.65 nm to be the (002). For the diffractions on the equator, the lowest angle diffraction of 1.79 nm and the strongest diffraction of 0.48 nm are assigned to be the (100) and (040), respectively. Careful structural analysis gives rise to a monoclinic unit cell with dimensions of a = 1.84 nm, b = 1.97 nm, c = 1.29 nm, $\alpha = \beta = 90°$, and $\gamma = 103.5°$ via the refinement. Table 2 lists the experimentally observed and calculated 2θ angles and d-spacing

Table 2. Crystallographic Parameters of DP8-PPV

	2θ (deg)		d-spacing (nm)		intensity	
(hkl) plane	expt[a]	calcd[b]	expt[a]	calcd[b]	expt[c]	simu[d]
100	4.9	4.9	1.79	1.79	vs	vs
110	7.5	7.5	1.18	1.18	s	s
−120	9.4	9.4	0.94	0.94	vw	w
111	10.2	10.2	0.87	0.87	vw	w
−130	13.5	13.6	0.66	0.65	vw	w
002	13.7	13.7	0.65	0.65	s	m
130	15.8	15.8	0.56	0.56	vw	vw
040	18.5	18.5	0.48	0.48	vs	s
−132	19.2	19.3	0.46	0.46	w	–
410	21.3	21.4	0.42	0.42	m	vw
113	21.9	22.0	0.41	0.40	vs	s
042	23.0	23.1	0.39	0.38	m	–
−133	24.7	24.8	0.36	0.36	vw	–

[a]Experimental values observed in Figure 4. [b]Calculated values based on the monoclinic unit cell of a = 1.84 nm, b = 1.97 nm, c = 1.29 nm, $\alpha = \beta = 90°$, $\gamma = 103.5°$. [c]The experimental intensities in Figure 4 and. [d]The simulated intensities in Figure 8 are semiquantitatively estimated and classified as very strong (vs), strong (s), medium (m), weak (w), and very weak (vw).

values based on this unit cell lattice. The calculated crystallographic density is 1.07 g/cm^3 with 4 chains (8 chemical repeat units) in each unit cell, slightly larger than the experimentally measured density of 1.06 g/cm^3. In addition, the crystal structure was also confirmed by SAED experimental results (see the Supporting Information).

The 2D WAXD patterns of DP10-PPV and DP12-PPV are shown in Figure 4, parts c and d, respectively, and their SAED results are shown in the Supporting Information. The diffractions in Figure 4, parts c and d, become fewer in number and more diffusive in comparison with that of oriented DP6-PPV and DP8-PPV. Seemingly, with increasing the length of alkyl side-chains (i.e., the value of n), DPn-PPV gradually losses the three-dimensionally positional order to a certain extent, and appears to be more liquid crystal-like. For DP10-PPV, a pair of strong diffraction arcs appears at the lowest angle of $2\theta = 4.8°$ (d = 1.84 nm) on the equator. In addition, other two pairs of diffractions at $2\theta = 9.6°$ (d = 0.92 nm) and $2\theta = 14.5°$ (d = 0.61 nm) can be observed (Figure 4c). They can be assigned as the (100), (200), and (300) diffraction, indicating a long-range ordered layer structure with its layer normal perpendicular to the chain axis. This is very similar to that observed in a smectic liquid crystalline phase. For DP12-PPV, the lowest angle diffraction is at $2\theta = 4.7°$ on the equator (Figures 4d), which should represent the (100) diffraction of a layer structure. However, there is no higher order diffraction detected, indicating that the layer structure does not possess a long-range order along the lateral direction of the conjugate backbone.

Although the crystalline order of DP10-PPV and DP12-PPV is largely decreased, we can still observe that the diffractions of 0.65 and 0.48 nm, which are characteristic for our DPn-PPV, appear on the meridian and equator, respectively. Again, these two can be assigned to the (002) and (040) diffraction. On the basis of the 2D WAXD and SAED results, the crystal structures of DP10-PPV and DP12-PPV are determined to be monoclinic via the refinement of the reciprocal lattices. For DP10-PPV, a = 1.98 nm, b = 2.05 nm, c = 1.29 nm, $\alpha = \beta = 90°$, and $\gamma = 111.4°$. For DP12-PPV, a = 2.14 nm, b = 2.21 nm, c = 1.29 nm, $\alpha = \beta =$

dx.doi.org/10.1021/ma302082x | Macromolecules 2013, 46, 155−163

Table 3. Crystal System, Axial System, and Density of DP*n*-PPV

		axial system						density (g/cm^3)	
sample	crystal system	a (nm)	b (nm)	c (nm)	α(deg)	β(deg)	γ (deg)	calcd	expt
DP6-PPV	orthorhombic	1.61	1.92	1.29	90	90	90	1.13	1.10
DP8-PPV	monoclinic	1.84	1.97	1.29	90	90	103.5	1.07	1.06
DP10-PPV	monoclinic	1.98	2.05	1.29	90	90	111.4	1.07	1.06
DP12-PPV	monoclinic	2.14	2.21	1.29	90	90	119.5	1.06	1.05

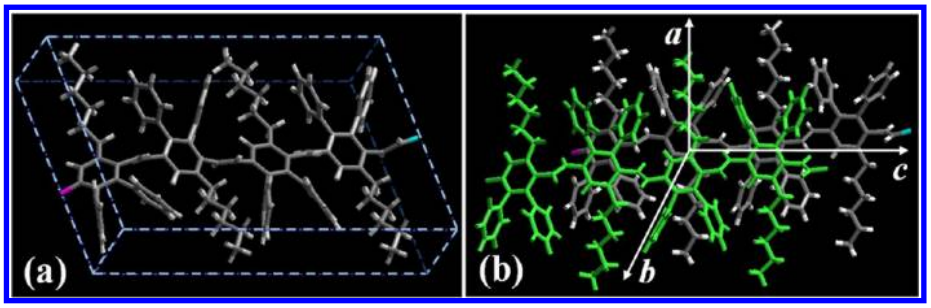

Figure 6. (a) Single chain conformation of DP6-PPV simulated by Cerius^2 after energy minimization. (b) Schematic illustration of the packing of two neighboring chains. The face-to-face stacking of two lath-like DP6-PPV chains occurs on the *b*-axis; the longitudinal and transverse displacement are along the *c*- and *a*-axis, respectively.

90°, and γ = 119.5°. The experimental and calculated 2θ angles and *d*-spacing values of the crystal lattice are listed in the Supporting Information.

Molecular Packing Scheme of DP*n*-PPVs in Crystals. Table 3 summarizes the lattice and density parameters of the four DP*n*-PPVs studied. While DP6-PPV unit cell is orthorhombic, other three samples have their unit cell of monoclinic. All of the four samples possess an identical *c*-axis dimension. On the other hand, the lattice parameters of *a*, *b*, and γ are systematically increased with the length of alkyl side-chain. As shown in Figures 3 and 4, the diffraction patterns of these four DP*n*-PPV samples look apparently quite different from each other. However, the results of crystal structure determinations suggest that the samples should share an identical basic chain packing behavior, which is little affected by varying the length of alkyl side-chain. To understand how the DP*n*-PPV molecules pack in the crystal, one of the key issues is to investigate the chain conformation.

It is known that the dominant driving force of crystallization of pristine PPV and many of its derivatives is the strong $\pi-\pi$ interaction of the conjugated moieties in the chains. The PPV backbones are planar and can stack parallel to maximize the $\pi-\pi$ interaction. DP*n*-PPV bears dominantly a *trans*-vinylene structure, as evidenced by the NMR experiment reported.[34] It is important to note that the *c* parameter of 1.29 nm of DP*n*-PPV corresponds to the length of two repeating units of PPV backbone. The PPV backbone of our samples should remain extended despite its slighted twisting due to the attached pendant groups, and therefore, it is still roughly planar. On the other hand, the two phenyl substituents can introduce significantly steric interaction along the backbone. As a result, the two adjacent repeating units within the chain have to arrange the phenyl groups on two opposite sides of the backbone in order to minimize the steric interaction in the crystal. Accordingly, the alkyl side-chains, which are also linked to the phenyl groups on the backbone, should extend to opposite directions alternatively with respect to the chain axis. The above considerations have been used to construct the chain model by utilizing the Cerius^2 software package. As an example, Figure 6a describes the simulation result of DP6-PPV single chain (four chemical repeating units) after energy minimization. Overall, the chain can be viewed as lath-like. The long axis of the molecular "lath" is the DP*n*-PPV backbone. On the other hand, the extended alkyl side-chain is nearly perpendicular to the backbone, determining the "lath" width; the planes of the substituent phenyls are largely orthogonal to backbone plane, giving the thickness of the "lath".

We found that stacking of lath-like DP*n*-PPV molecules could be applied to interpret the diffraction results. For DP6-PPV, the "lath" width is almost identical to the *a* parameter of the orthorhombic lattice. For other DP*n*-PPVs, a similar relationship can be obtained. This correlation suggests that the (100) diffraction of DP*n*-PPV is caused by the PPV backbones separated from each other, with the distance determined by the alkyl side-chains. When forming the crystal structure, the molecular "lathes" stack parallel fact-to-face. While their long axis (i.e., the chain axis) is along the *c*-axis, the alkyl side-chains largely intend to parallel to the *a*-axis, leading to the *a* parameter increased with the alkyl length. As mentioned above, the (040) diffraction of all the DP*n*-PPVs studied shares a same *d*-spacing of 0.48 nm. Therefore, the d_{010} (i.e., $b \sin \gamma$) is in fact a constant in disregard of the variance of *n*. The (040) diffraction is very strong in the 2D WAXD patterns (see Figure 4), which shall come from the face-to-face molecular packing along the normal of the "lath" surface (or the normal of backbone plane). It is worthy to mention here, for PPV and its derivatives without introduction of two phenyl rings as the pendant groups, the parallel packing due to the strong $\pi-\pi$ interaction of conjugated backbones results in the $\pi-\pi$ plane distance ranging from 0.35 to 0.40 nm, significantly smaller than the d_{040} of DP*n*-PPV.[17−20,22,30] This comparison indicates that the two phenyl groups of DP*n*-PPV in fact leads to distortion of the $\pi-\pi$ stacking of conjugated backbones.

Compared this series of PPV with other PPV derivatives, the four DP*n*-PPVs possess remarkably larger crystal lattice, which should be caused by the longitudinal (along the chain direction) and transverse offset of chain packing. Figure 6b shows that two parallel stacked chains of DP6-PPV with the

dx.doi.org/10.1021/ma302082x | *Macromolecules* 2013, 46, 155−163

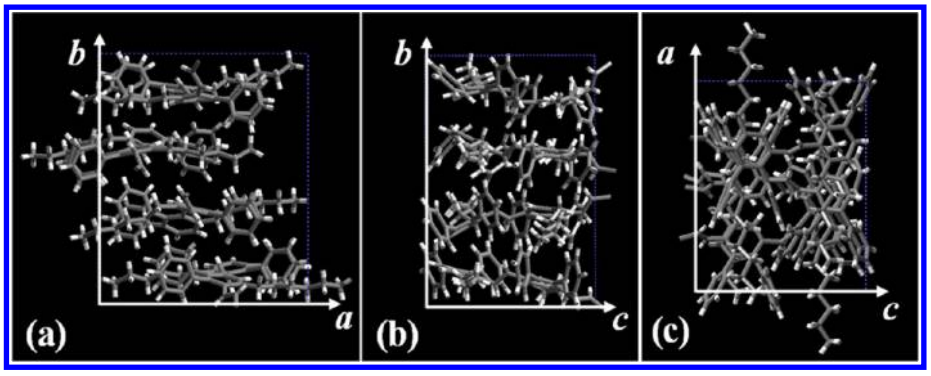

Figure 7. Molecular packing scheme of DP6-PPV in the unit cell simulated by Cerius[2]. The views are along the zone directions of (a) [001], (b) [100], and [010], respectively.

longitudinal displacement of one chemical repeating unit length. Obviously, such a displacement can greatly reduce the steric hindrance due to the interaction between the phenyl substituents of the neighboring chains, and thus the chains can pack more closely. As a result, electron densities of the (00*l*) planes for *l* = odd and even are identical. We consider that the *trans* conformation of single chain (Figure 6a) and the longitudinal offset of chain packing (Figure 6b) shall be the reason to account for the extinctions of the (00*l*) diffractions with *l* = odd. The transverse offset of the DP*n*-PPV chains in the lattice is also governed by the requirement of maximizing the $\pi-\pi$ interaction and minimizing the steric hindrance, which takes place along the *a*-axis (Figure 6b). Similar offsets of a shape-persistent polyhedral-oligosilsesquioxane-nanoparticle-tethered perylene diimide molecule are reported by us recently.[47]

On the basis of the lattice dimension and the density measured, we propose that each unit cell of DP*n*-PPV contains four chains. Figure 7 presents the molecular packing simulation result of DP6-PPV that can generate the diffraction pattern showing the best fit with the experimental observation. Starting from the perfect face-to-face packing of bare backbone, a series of complex offsets of the polymer chains is induced. As mentioned above, the neighboring chains glide halfway (~0.65 nm) to each other along the *c*-axis. The transverse displacements are then introduced along the lateral direction of the conjugate backbone, i.e., along the *a*-axis. With the attempt of maintaining the long-range order of the layer structure along the *b*-axis and also minimizing the long spacing period with the translational symmetry, we tried different displacements of the four DP6-PPV chains in the unit cell. The best displacements of the four chains can be found at 0.00, 0.25, 0.50, and 0.25 nm, respectively, which can fulfill the *b*-axis dimension of 1.92 nm and give the simulated diffraction pattern most close to the experimental data. Similarly, the molecular packing scheme can be simulated for other three DP*n*-PPVs with monoclinic structure, of which the results are shown in the Supporting Information.

The molecular packing scheme obtained by simulation further served as a model system to simulate the 2D WAXD fiber pattern. Figure 8 provides the simulated 2D WAXD patterns of the four DP*n*-PPVs, with the assumption that the chain orientation is not perfect. The semiquantitative comparison between the experimental and simulated diffraction intensities of the DP*n*-PPVs are summarized in Table 1, Table 2, and also Table S1 and Table S2 in the Supporting Information, respectively. The simulated diffraction results

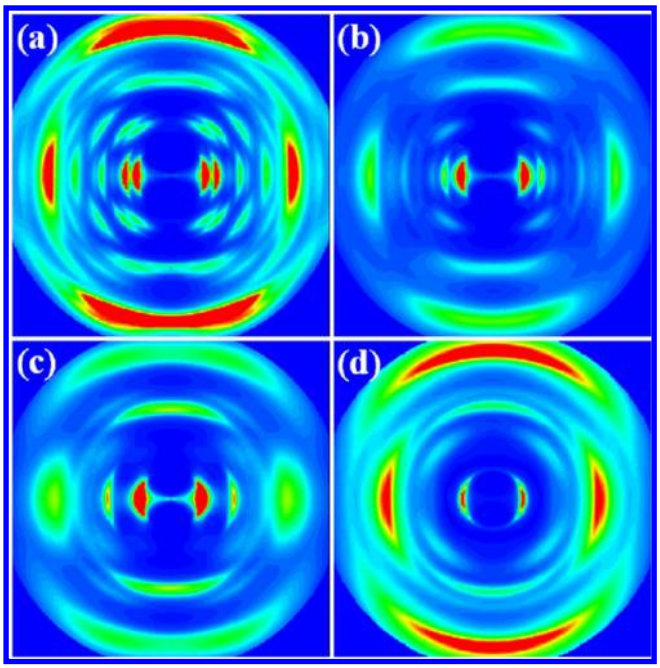

Figure 8. Simulated 2D WAXD patterns of DP*n*-PPVs: (a) *n* = 6; (b) *n* = 8; (c) *n* = 10; (d) *n* = 12. The chain axis (*c*-axis) is on the meridian.

agree fairly with our experimental results. The simulation confirms that the extinction of (001) and (003) diffraction arcs on the meridian is due to the longitudinal displacement of chains. On the other hand, the (100) and (040) diffraction locate at the position identical to that observed in experiments. According to the simulated molecular packing, we found that the longer alkyl side-chains contained more gauche configuration, and were not strictly parallel to each other in the unit cell (see the Supporting Information). This may be one of the reasons to account for the exhibited fewer in number and more diffused diffractions in DP10-PPV and DP12-PPV. Careful comparison can reveal some deviations between the experimental and simulated diffraction pattern. For example, the (101) diffraction showing in Figure 8a is absent in Figure 4a. This may be due to that the existence of chain defects such as head-to-head linkage which can cause the low degree of crystallinity and crystal defects. Overall, we consider that the molecular packing scheme proposed and simulated here have caught the essential features of chain packing behaviors of DP*n*-PPVs in their crystal structures.

dx.doi.org/10.1021/ma302082x | *Macromolecules* 2013, 46, 155−163

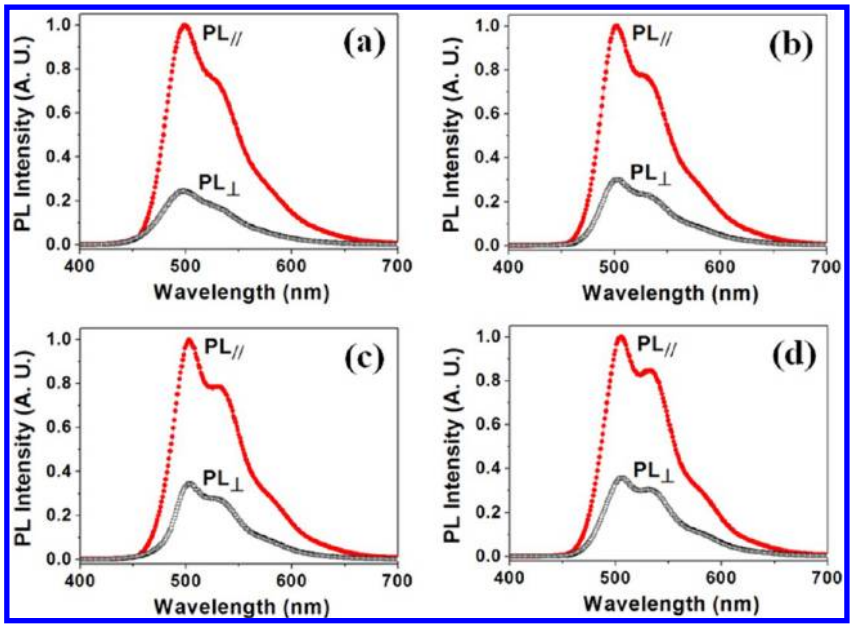

Figure 9. Polarized PL spectra of oriented film of DP*n*-PPVs: (a) n = 6; (b) n = 8; (c) n = 10; (d) n = 12.

Polarized Photoluminescence Properties. Encouraged by the 2D WAXD and simulation results that show the extended DP*n*-PPV chains can be highly aligned along the shear direction, we further studied the polarized PL property of the oriented DP*n*-PPV films. The shear induced alignment could be clearly visualized under PLM and also detected by polarized UV−vis absorption (see the Supporting Information). Since the transition moment of the lowest singlet exciton associated with the $\pi-\pi^*$ band gap is parallel to the backbone in conjugated polymers, one can use polarized light to probe the structural anisotropy in the films. The polarized UV−vis spectra showed different profiles depending on the type of polarization. A significantly larger absorption ascribed to the $\pi-\pi^*$ transition could be seen when the incident light was polarized parallel to the shear direction. The dichroic ratio of absorption ($D_{abs} = A_{\parallel}/A_{\perp}$) was estimated to be 2.9, 2.4, 1.9, and 1.8 for DP6-PPV, DP8-PPV, DP10-PPV, and DP12-PPV, respectively. Namely, the DP*n*-PPV sample with the shorter alkyl side-chain exhibits the higher D_{abs}. This tendency is in accordance with the value of T_g decreasing with increasing the alkyl side-chain length of DP*n*-PPV (see Figure 1). We presume that the sample with higher T_g may retain the orientation better after mechanical shearing.

The alignment of DP*n*-PPV backbones can give quite good polarized PL properties. The dichroic PL spectra of the films are shown in Figure 9, indicating that the light emitted from the oriented films was preferentially polarized parallel to the shear direction. The dichroic ratio of PL ($D_{PL} = I_{\parallel}/I_{\perp}$) is 4.0, 3.3, 2.9, and 2.7 for DP6-PPV, DP8-PPV, DP10-PPV, and DP12-PPV, respectively. Note that the D_{PL} values of DP*n*-PPVs are much higher than those of dialkoxy side-chain liquid crystalline PPVs ($D_{PL} \sim 1.2-1.4$)[48,49] and DP-PPV derivatives with mesogenic side groups ($D_{PL} \sim 1.5$).[35] The lower D_{PL} of DP*n*-PPVs containing the longer alkyl side chain may also arise from the lower T_g which allows the chains to relax more after shearing. On the other hand, the higher dichroism in PL than in absorption may be consistent with the migration of excitons to the lowest energy, most highly oriented segments of the polymer before emission occurred.[12,13] Considering the high solid state PL efficiency and high polarized emission dichroic ratio, DP*n*-PPV is expected to have the potential for polarized luminescence device applications.

CONCLUSIONS

In summary, the phase behavior and crystal structure of four DP*n*-PPV samples with flexible alkyl side-chains have been studied using a variety of techniques. On the basis of the 2D WAXD and SAED results obtained from the oriented samples, the crystal structures are determined to be orthorhombic for DP6-PPV and monoclinic for DP8-PPV, DP10-PPV, and DP12-PPV. The unit cell of DP*n*-PPV containing 4 chains (8 chemical repeat units) is remarkably larger in comparison with that of pristine PPV and other PPV derivatives. We consider that the DP*n*-PPV molecule is lath-like as a whole, which can stack face-to-face to form the crystal structure. The *a*-axis dimension is nearly identical to twice of the length of alkyl side-chain with extended conformation. The four parallel stacked lath-like chains in the unit cell possess transverse offset along the *a*-axis, resulting in a large *b*-axis dimension. On the other hand, the *c* parameter is equal to the length of two chemical repeating units along the extended PPV backbone. The longitudinal offset along the *c*-axis of the *trans* DP*n*-PPV in fact causes the extinction of (00*l*) diffraction with l = odd. The complex offsets of chain packing shall be attributed to both the maximization of interchain interaction and the minimization of steric hindrance caused by the substituted phenyl groups and alkyl chains. The molecular packing scheme of the DP*n*-PPV crystal was simulated utilizing crystallographic Cerius[2] software package. The simulated diffraction data agree with the diffraction results observed in the WAXD and SAED experiments. We also preliminarily studied the polarized PL property of the oriented DP*n*-PPV films. The dichroic PL spectra of the oriented films indicate that the light emitted from the oriented film was preferentially polarized parallel to the shear direction. The sample with shorter alkyl side-chain can exhibit higher dichroic ratio of PL. We expect that DP*n*-PPV has the potential application for linearly polarized luminescence devices.

dx.doi.org/10.1021/ma302082x | *Macromolecules* 2013, 46, 155−163

■ ASSOCIATED CONTENT

Supporting Information

TEM bright field images, SAED patterns, polarized UV−vis spectra and POM images of the oriented DP*n*-PPV film, two tables of crystallographic parameters of DP10-PPV and DP12-PPV, and molecular packing schemes simulated by Cerius^2 software. This material is available free of charge via the Internet at http://pubs.acs.org.

■ AUTHOR INFORMATION

Corresponding Author

*E-mail: (E.-Q.C.) eqchen@pku.edu.cn; (C.-S.H.) cshsu@mail.nctu.edu.tw.

Notes

The authors declare no competing financial interest.

■ ACKNOWLEDGMENTS

The authors thank Prof. Stephen Z. D. Cheng at the University of Akron for helpful and insightful discussions. This work was supported by the National Natural Science Foundation of China (20990232, 21074003, and 21104001).

■ REFERENCES

(1) Burroughes, J. H.; Bradley, D.; Brown, A. R.; Marks, R. N.; Mackay, K.; Friend, R. H.; Burns, P. L.; Holmes, A. B. *Nature* **1990**, *347*, 539−541.

(2) Friend, R. H.; Gymer, R. W.; Holmes, A. B.; Burroughes, J. H.; Marks, R. N.; Taliani, C.; Bradley, D.; Dos Santos, D. A.; Bredas, J. L.; Logdlund, M.; Salaneck, W. R. *Nature* **1999**, *397*, 121−128.

(3) Braun, D.; Heeger, A. J. *Appl. Phys. Lett.* **1991**, *58*, 1982−1984.

(4) Yang, S. H.; Hsu, C. S. *J. Polym. Sci., Polym. Chem.* **2009**, *47*, 2713−2733.

(5) Bao, Z. N.; Lovinger, A. J. *Chem. Mater.* **1999**, *11*, 2607−2612.

(6) Bahtiar, A.; Koynov, K.; Mardiyati, Y.; Horhold, H. H.; Bubeck, C. *J. Mater. Chem.* **2009**, *19*, 7490−7497.

(7) Cheng, Y. J.; Yang, S. H.; Hsu, C. S. *Chem. Rev.* **2009**, *109*, 5868−5923.

(8) Akcelrud, L. *Prog. Polym. Sci.* **2003**, *28*, 875−962.

(9) Hamaguchi, M.; Yoshino, K. *Appl. Phys. Lett.* **1995**, *67*, 3381−3383.

(10) Jandke, M.; Strohriegl, P.; Gmeiner, J.; Brutting, W.; Schwoerer, M. *Adv. Mater.* **1999**, *11*, 1518−1521.

(11) Molenkamp, W. C.; Watanabe, M.; Miyata, H.; Tolbert, S. H. *J. Am. Chem. Soc.* **2004**, *126*, 4476−4477.

(12) Grell, M.; Bradley, D. *Adv. Mater.* **1999**, *11*, 895−905.

(13) Nagamatsu, S.; Misaki, M.; Chikamatsu, M.; Kimura, T.; Yoshida, Y.; Azumi, R.; Tanigaki, N.; Yase, K. *J. Phys. Chem. B* **2007**, *111*, 4349−4354.

(14) Campoy-Quiles, M.; Ishii, Y.; Sakai, H.; Murata, H. *Appl. Phys. Lett.* **2008**, *92*, 213305(1−3).

(15) Gagnon, D. R.; Capistran, J. D.; Karasz, F. E.; Lenz, R. W. *Polym. Bull.* **1984**, *12*, 293−298.

(16) Capaz, R. B.; Caldas, M. J. *Phys. Rev. B* **2003**, *67*, 205205(1−9).

(17) Granier, T.; Thomas, E. L.; Gagnon, D. R.; Karasz, F. E.; Lenz, R. W. *J. Polym. Sci., Polym. Phys.* **1986**, *24*, 2793−2804.

(18) Chen, D.; Winokur, M. J.; Masse, M. A.; Karasz, F. E. *Polymer* **1992**, *33*, 3116−3122.

(19) Chen, D.; Winokur, M. J.; Masse, M. A.; Karasz, F. E. *Phys. Rev. B* **1990**, *41*, 6759−6767.

(20) Zhang, X. B.; Vantendeloo, G.; Vanlanduyt, J.; Vandijck, D.; Briers, J.; Bao, Y.; Geise, H. J. *Macromolecules* **1996**, *29*, 1554−1561.

(21) Chen, S. H.; Su, A. C.; Chou, H. L.; Peng, K. Y.; Chen, S. A. *Macromolecules* **2004**, *37*, 167−173.

(22) Chen, S. H.; Su, A. C.; Han, S. R.; Chen, S. A.; Lee, Y. Z. *Macromolecules* **2004**, *37*, 181−186.

(23) Babudri, F.; Cicco, S. R.; Farinola, G. M.; Naso, F.; Bolognesi, A.; Porzio, W. *Macromol. Rapid Commun.* **1996**, *17*, 905−911.

(24) Olsen, B. D.; Jang, S. Y.; Luning, J. M.; Segalman, R. A. *Macromolecules* **2006**, *39*, 4469−4479.

(25) Jeng, U.; Hsu, C. H.; Sheu, H. S.; Lee, H. Y.; Inigo, A. R.; Chiu, H. C.; Fann, W. S.; Chen, S. H.; Su, A. C.; Lin, T. L.; Peng, K. Y.; Chen, S. A. *Macromolecules* **2005**, *38*, 6566−6574.

(26) Resel, R.; Tertinek, B.; Tasch, S.; Davey, A.; Blau, W.; Horhold, H. H.; Rost, H.; Leising, G. *Synth. Met.* **1999**, *101*, 96−97.

(27) Resel, R.; Kiebooms, R.; Vanderzande, D.; Stelzer, F. *Monatsh. Chem.* **2001**, *132*, 433−440.

(28) Martens, J.; Marseglia, E. A.; Bradley, D.; Friend, R. H.; Burn, P. L.; Holmes, A. B. *Synth. Met.* **1993**, *55*, 449−453.

(29) Gill, R. E.; Meetsma, A.; Hadziioannou, G. *Adv. Mater.* **1996**, *8*, 212−214.

(30) Yang, C. Y.; Hide, F.; Diaz-Garcia, M. A.; Heeger, A. J.; Cao, Y. *Polymer* **1998**, *39*, 2299−2304.

(31) Olsen, B. D.; Alcazar, D.; Krikorian, V.; Toney, M. F.; Thomas, E. L.; Segalman, R. A. *Macromolecules* **2008**, *41*, 58−66.

(32) Hsieh, B. R.; Yu, Y.; Forsythe, E. W.; Schaaf, G. M.; Feld, W. A. *J. Am. Chem. Soc.* **1998**, *120*, 231−232.

(33) Hsieh, B. R.; Wan, W. C.; Yu, Y.; Gao, Y. L.; Goodwin, T. E.; Gonzalez, S. A.; Feld, W. A. *Macromolecules* **1998**, *31*, 631−636.

(34) Wu, Y. C.; Ren, X. K.; Chen, E. Q.; Lee, H. M.; Duvail, J. L.; Wang, C. L.; Hsu, C. S. *Macromolecules* **2012**, *45*, 4540−4549.

(35) Li, A. K.; Yang, S. S.; Jean, W. Y.; Hsu, C. S.; Hsieh, B. R. *Chem. Mater.* **2000**, *12*, 2741−2744.

(36) Yang, S. H.; Li, H. C.; Chen, C. K.; Hsu, C. S. *J. Polym. Sci., Polym. Chem.* **2006**, *44*, 6738−6749.

(37) Yang, S. H.; Chen, S. Y.; Wu, Y. C.; Hsu, C. S. *J. Polym. Sci., Polym. Chem.* **2007**, *45*, 3440−3450.

(38) Liao, Y. M.; Shih, H. M.; Hsu, K. H.; Hsu, C. S.; Chao, Y. C.; Lin, S. C.; Chen, C. Y.; Meng, H. F. *Polymer* **2011**, *52*, 3717−3724.

(39) Li, Y. C.; Chen, K. B.; Chen, H. L.; Hsu, C. S.; Tsao, C. S.; Chen, J. H.; Chen, S. A. *Langmuir* **2006**, *22*, 11009−11015.

(40) Li, Y. C.; Chen, C. Y.; Chang, Y. X.; Chuang, P. Y.; Chen, J. H.; Chen, H. L.; Hsu, C. S.; Ivanov, V. A.; Khalatur, P. G.; Chen, S. A. *Langmuir* **2009**, *25*, 4668−4677.

(41) Lukyanov, A.; Malafeev, A.; Ivanov, V.; Chen, H. L.; Kremer, K.; Andrienko, D. *J. Mater. Chem.* **2010**, *20*, 10475−10485.

(42) Eashoo, M.; Wu, Z. Q.; Zhang, A. Q.; Shen, D. X.; Tse, C.; Harris, F. W.; Cheng, S. Z. D.; Gardner, K. H.; Hsiao, B. S. *Macromol. Chem. Phys.* **1994**, *195*, 2207−2225.

(43) Cheng, S. Z. D. Phase Transitions in Polymers: The Role of Metastable States; Elsevier: Amsterdam, 2008.

(44) Jing, A. J.; Taikum, O.; Li, C. Y.; Harris, F. W.; Cheng, S. Z. D. *Polymer* **2002**, *43*, 3431−3440.

(45) Ge, J. J.; Zhang, A. Q.; Mccreight, K. W.; Ho, R. M.; Wang, S. Y.; Jin, X. M.; Harris, F. W.; Cheng, S. Z. D. *Macromolecules* **1997**, *30*, 6498−6506.

(46) Ruan, J. J.; Ge, J. J.; Zhang, A. Q.; Shi, J.; Wang, S. Y.; Harris, F. W.; Cheng, S. Z. D. *Macromolecules* **2002**, *35*, 736−745.

(47) Ren, X. K.; Sun, B.; Tsai, C. C.; Tu, Y. F.; Leng, S. W.; Li, K. X.; Kang, Z.; Van Horn, R. M.; Li, X. P.; Zhu, M. F.; Wesdemiotis, C.; Zhang, W. B.; Cheng, S. Z. D. *J. Phys. Chem. B* **2010**, *114*, 4802−4810.

(48) Kijima, M.; Akagi, K.; Shirakawa, H. *Synth. Met.* **1997**, *84*, 237−238.

(49) Akagi, K.; Oguma, J.; Shibata, S.; Toyoshima, R.; Osaka, I.; Shirakawa, H. *Synth. Met.* **1999**, *102*, 1287−1288.